

Highlights

Hybrid Quantum-Classical Autoencoders for Unsupervised Network Intrusion Detection

Mohammad Arif Rasyidi, Omar Alhussein, Sami Muhaidat, Ernesto Damiani

- We present a large-scale, systematic evaluation of hybrid quantum-classical (HQC) autoencoders for network intrusion detection systems (NIDS), iterating over key design choices, including quantum layer placement, measurement approach, variational and non-variational formulations, latent-space regularization, and the anomaly detection mechanism.
- We conduct a comprehensive ablation study across architectural and algorithmic dimensions. The study isolates two factors with consistent impact: early placement of the quantum layer and the use of reconstruction-error scores for anomaly detection.
- We find that unsupervised HQC models exhibit high sensitivity to architectural choices. However, when carefully configured, they often provide more stable and reliable detection on unseen attacks than both their classical supervised and unsupervised counterparts.
- We show that under strict zero-day scenarios, optimized HQC models demonstrate stronger generalization and lower performance variability than both classical unsupervised and supervised models.
- We assess HQC robustness under simulated quantum hardware imperfections. Simulated gate noise causes measurable reductions in AUROC, and the results define concrete requirements for noise-aware HQC design.

Hybrid Quantum-Classical Autoencoders for Unsupervised Network Intrusion Detection

Mohammad Arif Rasyidi^{a,*}, Omar Alhussein^{a,*}, Sami Muhaidat^a,
Ernesto Damiani^{b,a}

^a*6G Research Center, College of Computing and Mathematical Sciences, Khalifa
University, Abu Dhabi, United Arab Emirates*

^b*Università degli Studi di Milano, Milan, Italy*

Abstract

Unsupervised anomaly-based intrusion detection requires models that can generalize to attack patterns not observed during training. This work presents the first large-scale evaluation of hybrid quantum-classical (HQC) autoencoders for this task. We construct a unified experimental framework that iterates over key quantum design choices, including quantum-layer placement, measurement approach, variational and non-variational formulations, and latent-space regularization. Experiments across three benchmark NIDS datasets show that HQC autoencoders can match or exceed classical performance in their best configurations, although they exhibit higher sensitivity to architectural decisions. Under zero-day evaluation, well-configured HQC models provide stronger and more stable generalization than classical and supervised baselines. Simulated gate-noise experiments reveal early performance degradation, indicating the need for noise-aware HQC designs. These results provide the first data-driven characterization of HQC autoencoder behavior for network intrusion detection and outline key factors that govern their practical viability. All experiment code and configurations are available at <https://github.com/arasyi/hqcae-network-intrusion-detection>.

Keywords: anomaly detection, autoencoders, hybrid quantum-classical models, network intrusion detection systems (NIDS), quantum machine learning (QML)

*Corresponding authors.

Email addresses: 100066916@ku.ac.ae (Mohammad Arif Rasyidi),
omar.alhussein@ku.ac.ae (Omar Alhussein)

1. Introduction

The growing interconnectivity of modern systems has led to a rapid increase in network traffic, resulting in the emergence of more diverse and difficult-to-predict cyberattacks. In this context, network intrusion detection systems (NIDS) are crucial as primary line of defense in many organizations. Conventional NIDS generally still rely heavily on signature-based methods. While these methods are effective in detecting known threats, they are less capable of identifying novel or zero-day attacks (Guo, 2023; Sharma and Chen, 2024). This limitation has led to the development of anomaly-based detection approaches that study normal network behavior patterns and flag significant deviations as potential intrusions (Alsoufi et al., 2021; Zachos et al., 2021).

In recent years, deep learning has become a powerful tool for anomaly detection, as it can automatically learn complex features without the need for manual feature engineering (Vinayakumar et al., 2019). While early approaches often relied on recurrent neural networks (Yin et al., 2017), recent developments explore more complex architectures such as Transformers (Manocchio et al., 2024; Long et al., 2024; Chen et al., 2023) and graph neural networks (Zhong et al., 2024; Lo et al., 2022; Sun et al., 2024). While these models excel at capturing complex temporal and relational dependencies in network data, their application often assumes the availability of labeled data. In unsupervised anomaly detection scenario, the model can only learn from normal data without any examples of attacks, and therefore generally requires a different architecture than supervised methods. A well-known example is the autoencoder (AE) architecture, which has been proven to be particularly suitable for the task due to its unsupervised nature (Sakurada and Yairi, 2014; An and Cho, 2015). By learning to reconstruct normal data through a compressed latent space, AE directly addresses the problem of identifying anomalous samples via their high reconstruction error.

The basic autoencoder architecture has since inspired numerous variations. A notable extension is the variational autoencoder (VAE), which introduces a probabilistic latent space, making it a powerful generative model (Kingma and Welling, 2013). Further research has focused on improving the robustness of autoencoders, particularly in scenarios where training data may be contaminated with unlabeled anomalies, which is a very common

challenge in the real-world (Bouman and Heskes, 2025; Neloy and Turgeon, 2024). Techniques such as adding regularization terms to the loss function have been proposed to reduce the performance drop seen in these settings (Nkashama et al., 2024; Yu et al., 2021). These methods have helped extend the usefulness of classical autoencoders, but they also highlight their limits. As a result, researchers have begun exploring models with greater flexibility and representational capacity.

Currently, quantum computing has recently opened a promising direction for machine learning research (Biamonte et al., 2017). Although fault-tolerant quantum computers remain a future prospect, the current generation of noisy intermediate-scale quantum devices (NISQ) has motivated the development of variational quantum algorithms (VQAs) and hybrid quantum-classical models (HQC) (Preskill, 2018; Cerezo et al., 2021). These methods combine classical and quantum computation, relying on classical processors for most tasks while using quantum circuits for specific operations where they may offer an advantage. A common approach involves embedding a parameterized quantum circuit (PQC) as a layer within a classical deep learning network (Mitarai et al., 2018). The potential advantage of such a quantum layer lies in its ability to navigate and process information in the exponentially large Hilbert space of the quantum state, which potentially allows for more expressive feature representations than those accessible to purely classical models (Havlíček et al., 2019; Schuld et al., 2021).

Building on these developments, several studies have explored quantum techniques for NIDS. Existing work primarily follows two directions: native quantum machine learning (QML) classifiers, which utilize fully quantum or variational circuits for supervised intrusion detection (Gouveia and Correia, 2020; Abreu et al., 2024), and hybrid pipelines, that integrate classical autoencoders or feature extractors with quantum classifiers in supervised downstream stages (Hdaib et al., 2024). Although these approaches have shown promising improvements in classification accuracy and model size, they rely on labeled datasets and, as a result, have limited ability to detect novel or zero-day attacks. To the best of our knowledge, no previous work has investigated HQC autoencoders for fully unsupervised NIDS, where the model learns only from normal traffic patterns without labeled anomalies.

Beyond this methodological gap, the broader HQC literature remains largely at a proof-of-concept stage (Gouveia and Correia, 2020). Prior studies typically evaluate a single architecture on small or synthetic datasets (Sakhnenko et al., 2022; Hdaib et al., 2024), leaving open questions about

how architectural and algorithmic design choices influence performance. The HQC autoencoder design space is inherently large, encompassing the selection of (1) the classical backbone, (2) the structure and placement of quantum layers, (3) the method of encoding classical data into quantum states (which is known to be a crucial factor in expressivity (Schuld et al., 2021; LaRose and Coyle, 2020)), and (4) the scheme used to measure quantum output. Yet, no systematic analysis of the interaction of these factors or of which configurations produce robust and reliable performance exist.

To address this gap, we conduct a comprehensive evaluation of HQC autoencoders for unsupervised NIDS. Our unified framework explores key quantum design choices and compares HQC and classical models across three widely used benchmark datasets (UNSW-NB15, NSL-KDD, and CIC-IDS2017) which cover a broad range of network traffic characteristics and threat types (Moustafa and Slay, 2015; Tavallaei et al., 2009; Sharafaldin et al., 2018). Our analysis reveals two key findings: (i) unsupervised HQC models show notably higher performance variance across architectural configurations, which indicates strong sensitivity to quantum-layer placement and measurement strategy; and (ii) well-configured HQC models deliver more stable and reliable detection on unseen attack types compared to both their classical supervised and unsupervised model counterpart.

Building on these insights, our main contributions are as follows:

1. We establish a large-scale benchmark for HQC autoencoders in unsupervised NIDS. The benchmark study exposes clear dependencies on architectural design choices and dataset characteristics.
2. We conduct a comprehensive ablation study across architectural and algorithmic dimensions. The study isolates two factors with consistent impact: early placement of the quantum layer and the use of reconstruction-error scores for anomaly detection.
3. We show that under strict zero-day scenarios, HQC models demonstrate stronger generalization and lower performance variability than both classical unsupervised and supervised models.
4. We assess HQC robustness under simulated quantum hardware imperfections. Simulated gate noise causes measurable reductions in AUROC, and the results define concrete requirements for noise-aware HQC design.

The rest of this paper is organized as follows. Section 2 presents the relevant background on autoencoders and HQC models, reviews related lit-

erature, and positions our work. Section 3 describes our methodology. In Section 4, we present and discuss our findings. Finally, Section 5 concludes the paper with a summary and directions for future work.

2. Background and Related Work

In this section, we review the basic of AE architectures for anomaly-based NIDS and then survey the relevant classical and quantum literatures. We discuss the positioning of our work by identifying gaps in the comparative analysis of HQC architectures.

2.1. Classical Autoencoders for Unsupervised Anomaly Detection

The application of machine learning to NIDS has become a fairly well-established field. In particular, recent advances in deep learning have proven capable of reducing the reliance on manual feature engineering that characterized previous generation approaches (Asharf et al., 2020; Wu et al., 2024; Al Siam et al., 2025). Among these models, we focus on AEs, primarily due to their ability to learn representations of normal data without the need for labeled anomaly examples (Sakurada and Yairi, 2014; An and Cho, 2015).

An AE is a neural network with two components: an encoder and a decoder. The encoder, E , maps an input $\mathbf{x} \in \mathbb{R}^d$ to a lower-dimensional latent representation $\mathbf{z} = E(\mathbf{x})$, where $\mathbf{z} \in \mathbb{R}^k$ and $k < d$. The decoder, D , then attempts to reconstruct the original input, producing $\hat{\mathbf{x}} = D(\mathbf{z})$. The model is trained by minimizing the reconstruction error, typically the mean squared error (MSE), between the input and its reconstruction:

$$\mathcal{L}_{\text{recon}} = \|\mathbf{x} - \hat{\mathbf{x}}\|^2 = \|\mathbf{x} - D(E(\mathbf{x}))\|^2. \quad (1)$$

When trained solely on normal samples, AE learns a compressed representation of the normal data distribution. Anomalous samples with patterns different from the training data tend to be difficult to reconstruct well, resulting in higher reconstruction errors. This error value can then be used as an anomaly score and informs detection decisions (Sakurada and Yairi, 2014; An and Cho, 2015).

A notable AE variant is the VAE, which adopts a probabilistic approach (Kingma and Welling, 2013). The encoder in a VAE no longer generates a single latent point but instead learns the parameters of a probability distribution, usually a Gaussian distribution, and the latent vector \mathbf{z} is sampled

from that distribution. The VAE objective function consists of two parts, namely a reconstruction term and a Kullback-Leibler (KL) divergence term, which acts as a regularization term for the latent space:

$$\mathcal{L}_{\text{KL}} = D_{\text{KL}}(q(\mathbf{z}|\mathbf{x})||p(\mathbf{z})), \quad (2)$$

$$\mathcal{L}_{\text{VAE}} = \mathcal{L}_{\text{recon}} + \beta \cdot \mathcal{L}_{\text{KL}}. \quad (3)$$

Here, the hyperparameter β controls the balance between the reconstruction fidelity and the level of regularization imposed on the latent space. In this way, the VAE not only reconstructs the data but also forms a more regular latent structure.

A practical challenge for anomaly detection models is training data contamination by unlabeled anomalies. This can occur due to mislabeling recorded in various benchmark datasets (Liu et al., 2022; Pinto et al., 2025), or due to the highly heterogeneous nature of network traffic within classes considered benign (Guerra et al., 2022). If this contamination is large enough, the autoencoder can inadvertently learn to reconstruct malicious samples as if they are part of a normal pattern, and detection performance degrades significantly.

To improve resilience to this type of contamination, several recent works have proposed regularization techniques for the latent space (Yu et al., 2021; Nkashama et al., 2024). Our study incorporates a recent method by Nkashama et al. (2024), which introduces a latent space regularization term to the loss function. This approach introduces a learnable centroid parameter, $\boldsymbol{\mu}_c$, to the latent space, and then penalizes the distance between the latent representation of each training sample and the centroid:

$$\mathcal{L}_{\text{reg}} = \|\mathbf{z} - \boldsymbol{\mu}_c\|^2. \quad (4)$$

The idea behind this technique is to direct the representations of normal data to form tighter cluster. When the cluster becomes more compact, anomalous samples tend to fall farther from the center, which makes them easier to detect even when the training data is slightly contaminated.

2.2. Hybrid Quantum-Classical Models for NIDS

QML is an emerging field that seeks to apply quantum mechanical principles, such as superposition and entanglement, to computational problems. The leading paradigm for near-term devices is the VQA, which uses a classical optimizer to tune the parameters of a PQC within a hybrid loop (Cerezo

et al., 2021). This structure allows the PQC to be integrated as a layer within an artificial neural network, where its parameters are updated through a backpropagation process (Mitarai et al., 2018). The underlying motivation is the hypothesis that quantum layers exploit the exponentially large embedding of Hilbert spaces, enabling the modeling of correlations that remain difficult for equivalently sized classical architectures (Schuld et al., 2021; Jerbi et al., 2023). However, training is non-trivial and can be hampered by issues such as barren plateaus (Larocca et al., 2025). Furthermore, near-term quantum devices are susceptible to environmental noise and other open-system effects, which introduce errors into computation and can impact model performance.

The application of QML to cybersecurity is a rapidly developing field. Early research demonstrates feasibility with algorithms such as quantum support vector machines (Gouveia and Correia, 2020). More recent research has shifted toward HQC deep learning models, including hybrid autoencoders for anomaly detection across various domains (Sakhnenko et al., 2022; Ngairangbam et al., 2022; Frehner and Stockinger, 2025). As summarized in Table 1, quantum-based NIDS research has largely explored (i) supervised QML classifiers (Gouveia and Correia, 2020; Abreu et al., 2024) or (ii) hybrid pipelines that pair quantum autoencoders with downstream quantum classifiers (Hdaib et al., 2024).

In an unsupervised NIDS setting, a systematic and large-scale benchmark comparing different HQC autoencoder designs to equivalently-complex classical models is notably missing. Furthermore, the impact of fundamental architectural choices, such as quantum layer placement and measurement methods, on performance and generalization has not been systematically investigated. The practical implications of hardware noise on the performance of HQC autoencoders for NIDS are also still largely unquantified. Consequently, there is a lack of evidence-based guidance for practitioners looking to construct and deploy these models.

Table 1: Comparison of recent works on QML for NIDS.

Reference	Method	Learning Paradigm	Key Contribution / Finding
Gouveia and Correia (2020)	Quantum SVM	Supervised	Proof-of-concept for quantum-enhanced NIDS.
Hdaib et al. (2024)	HQC-AE + Q-Classifer	Hybrid	Explored combining QAE with downstream quantum models.
Abreu et al. (2024)	QML Classifiers	Supervised	Showed QML outperforming classical ML on NIDS datasets.
This Work	Classical & HQC AEs	Unsupervised (with supervised reference)	Systematic benchmark of HQC autoencoders for unsupervised NIDS, analyzing architectural factors, zero-day generalization, and noise sensitivity.

3. Methodology

In this section, we present the methodological framework we use to evaluate the proposed HQC autoencoder for NIDS. We describe the dataset selection and preprocessing steps, the model architecture, and the training configuration, followed by the anomaly detection mechanisms and the supervised baselines. We conclude with the experimental protocol, evaluation metrics, and hardware noise simulation, ensuring a systematic and reproducibility of the proposed approach.

3.1. Datasets and Preprocessing

To ensure the generality of our findings, we conduct experiments on three widely recognized NIDS datasets, each presenting distinct traffic characteristics and attack scenarios.

- **UNSW-NB15:** A contemporary dataset generated from a commercial network testbed, encompassing a mixture of normal activities and nine modern attack types. It is valued for its realism and complexity (Moustafa and Slay, 2015).
- **NSL-KDD:** An improved version of the seminal KDD’99 dataset, which addresses several of its inherent statistical issues. It remains a standard benchmark for comparing NIDS performance (Tavallaei et al., 2009).
- **CIC-IDS2017:** A comprehensive dataset containing up-to-date benign traffic and a variety of common attacks, such as Brute Force, DoS, and Web Attacks, captured over a five-day period (Sharafaldin et al., 2018).

A standardized preprocessing pipeline is applied to all datasets. Categorical features are encoded using one-hot encoding. All numerical features are subsequently scaled to have zero mean and unit variance fitted only on the training data. For UNSW-NB15 and NSL-KDD, the provided train/test split is used. For CIC-IDS2017, which does not provide an official train/test split, we first excluded the Monday capture, as it contains only benign traffic and would otherwise dominate the dataset without contributing attack diversity. From the remaining four days (Tuesday–Friday), we randomly sampled 5% of the combined traffic as the training set and used the remaining 95% for

testing. As in the other datasets, only samples labeled as normal within the training portion are used to train the unsupervised autoencoders, following standard practice for anomaly detection.

3.2. A Unified Autoencoder Framework

Our investigation focuses on four principal autoencoder architectures summarized in Fig. 1. All four are housed within a unified framework that encompasses both classical and HQC variants in a consistent design. In general, the encoder compresses an input \mathbf{x} into a latent representation \mathbf{z} . In AE, \mathbf{z} is deterministic, while in VAE, it is probabilistic. To achieve an HQC equivalent, we insert an optional quantum layer (QLayer) within this pipeline, so that each classical architecture has a comparable hybrid version.

We consider two QLayer placements. In the Early configuration, the QLayer operates on a classically transformed version of the input before significant dimensionality reduction takes place. In the Late configuration, the QLayer operates on an intermediate representation that is already lower-dimensional and closer to the latent space. After this mapping phase, the decoder reconstructs the output $\hat{\mathbf{x}}$ from \mathbf{z} , and completes the autoencoding process. In this way, the main differences between the architectures lie in the presence of the QLayer and its insertion position, while the basic encoder-decoder flow remains similar.

Although the layer structures differ, the learning objectives of the four architectures can be summarized in a single unified loss function. The total objective, $\mathcal{L}_{\text{total}}$, is expressed as the weighted sum of three components, namely

$$\mathcal{L}_{\text{total}} = \mathcal{L}_{\text{recon}} + \beta \cdot \mathcal{L}_{\text{KL}} + \alpha \cdot \mathcal{L}_{\text{reg}}. \quad (5)$$

The first component, $\mathcal{L}_{\text{recon}}$, represents the mean squared error between the input \mathbf{x} and its reconstruction $\hat{\mathbf{x}}$ as defined in Eq. (1). This term serves as the basic objective for all autoencoders in our framework. The second component, \mathcal{L}_{KL} , represents the KL divergence between the learned latent distribution and a standard normal prior, as defined in in Eq. (2). The hyperparameter β governs how strongly this probabilistic regularization is applied. When β is zero, the model reduces back to a regular autoencoder, while for β greater than zero, the model behaves as a variational autoencoder. The third and final component, \mathcal{L}_{reg} , is a latent regularization loss that penalizes the squared Euclidean distance between the latent representation \mathbf{z} and a learnable centroid $\boldsymbol{\mu}_c$, as defined in Eq. 4 and proposed by Nkashama et al.

(2024). The hyperparameter α determines whether this latent regularization is activated and how strong its effect is. By manipulating α and β , we can instantiate four primary model types: a standard AE ($\alpha = 0, \beta = 0$), a VAE ($\alpha = 0, \beta > 0$), an AE with latent regularization ($\alpha > 0, \beta = 0$), and a VAE with latent regularization ($\alpha > 0, \beta > 0$). This unified definition facilitates systematic comparisons across architectures in our study.

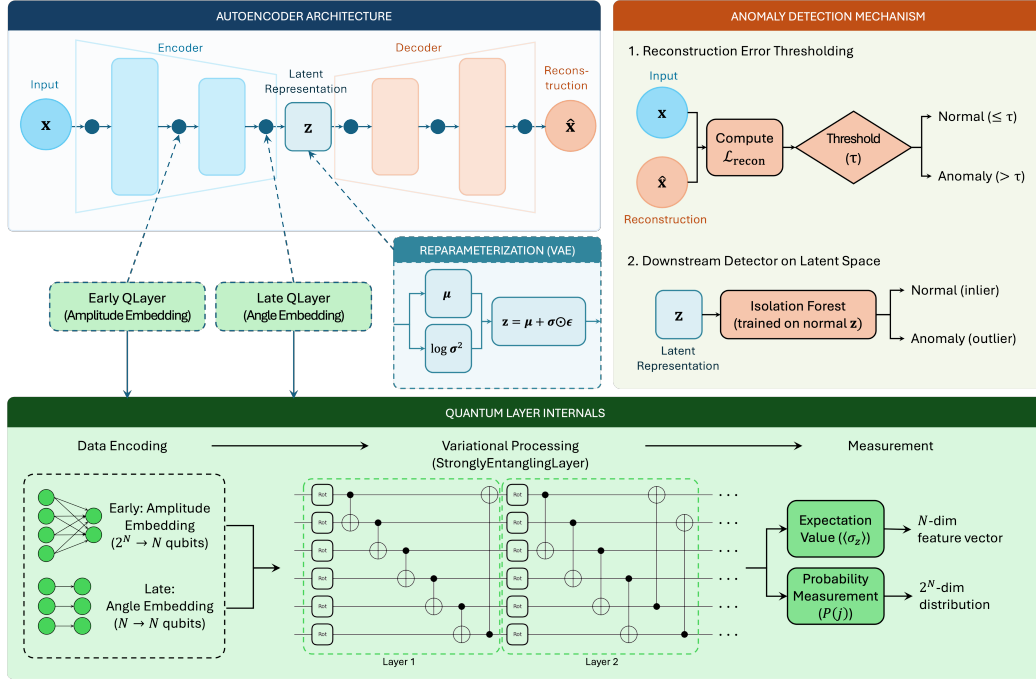


Figure 1: Unified HQC autoencoder architecture showing QLayer placement, internals, and anomaly detection mechanisms.

3.3. Hybrid Quantum-Classical Architecture Design

As illustrated in Fig. 1, the HQC configurations integrate a PQC denoted by the QLayer, within the encoder. The figure also outlines the internal steps of the QLayer: data encoding, variational processing, and measurement. The design of the encoding and measurement stages is especially important. For the encoding, we investigate two options depending on the QLayer's placement within the encoder.

1. **Early-Stage Quantum Layer.** Here, the QLayer is placed close to the encoder input. A classical layer first projects the input data to a

dimension of 2^N , where N is the number of qubits, making it suitable for amplitude embedding. The resulting vector \mathbf{x} is then encoded into the amplitude of the multi-qubit state $|\psi\rangle = \sum_{i=0}^{2^N-1} x_i|i\rangle$. This approach is efficient for encoding high-dimensional data, as 2^N features can be represented using only N qubits (Schuld et al., 2020, 2021).

2. **Late-Stage Quantum Layer.** In this setting, the QLayer is placed deeper within the encoder. Several classical layers process the input first. The output is then projected to an N -dimensional vector and encoded through angle embedding, where each feature drives a single-qubit rotation. This results in a more compact and hardware-efficient representation, suitable for near-term quantum devices (Mitarai et al., 2018).

The two strategies differ in both expressiveness and feasibility. Amplitude embedding provides higher information density but requires deeper circuits to prepare arbitrary states (Shende et al., 2006; Mottonen et al., 2004). Angle embedding, while less expressive, tends to produce much shallower circuits and is therefore often considered more suitable for current devices (Havlíček et al., 2019). Our experiments therefore compare these approaches to understand the trade-off between representational power and practical implementation on NISQ hardware.

Following the data encoding step, the quantum state evolves through a variational ansatz. We adopt a hardware-efficient ansatz with full entangling layers, known for its high expressivity and ability to generate strong entanglement between qubits (Schuld et al., 2020). The trainable parameters of this ansatz are optimized along with the classical network weights through backpropagation. To return to the classical domain, the final quantum state $|\psi_f\rangle$ is measured using one of two readout schemes:

1. **Expectation Value Measurement.** Here, we compute the expectation value of the Pauli-Z observable $\sigma_{z,i}$ for each qubit i ,

$$\langle\sigma_{z,i}\rangle = \text{Tr}(\sigma_{z,i}|\psi_f\rangle\langle\psi_f|), \quad (6)$$

where $|\psi_f\rangle$ denotes the final quantum state vector, $\langle\psi_f|$ its conjugate transpose, and Tr the trace operation. This process yields a compact, N -dimensional real-valued feature vector.

2. **Probability Measurement.** The final quantum state $|\psi_f\rangle$ is measured in the computational basis $\{|0\rangle, |1\rangle\}^{\otimes N}$. This measurement yields

a 2^N -dimensional probability distribution $P(j)$ over all basis states $|j\rangle$. The probabilities are given by

$$P(j) = |\langle j | \psi_f \rangle|^2. \quad (7)$$

This distribution provides a richer description of the final quantum state, but comes at a higher computational cost because the number of probability components grows exponentially with the number of qubits.

3.4. Anomaly Detection Mechanisms

Once an autoencoder model is trained on normal data, we employ two distinct mechanisms to classify the new, unseen samples.

1. **Reconstruction Error Thresholding:** This is the most direct method for anomaly detection with autoencoders. For each sample in the test set, we compute its reconstruction error. A detection threshold, τ , is established by calculating the 95th percentile of the reconstruction errors observed on the normal training data. A test sample is classified as an anomaly if its reconstruction error exceeds this threshold τ .
2. **Downstream Detector on Latent Space:** The trained encoder is used as a feature extractor that transforms the high-dimensional input data into its compact latent representation. A separate, unsupervised anomaly detection algorithm, namely the isolation forest (Liu et al., 2008), is then trained exclusively on the latent representations of the normal training data. This trained model is subsequently used to classify the latent representations of the test data as either normal (inlier) or anomaly (outlier).

3.5. Supervised Baseline Configuration

To establish comparative baselines on detection performance, a supervised model is developed using the encoder component of the classical autoencoder architecture. A single dense output neuron with a sigmoid activation function is appended to produce a probabilistic binary classification output, corresponding to the likelihood of a network flow instance being anomalous or benign. The model parameters are optimized using binary cross-entropy loss and the Adam optimizer under identical preprocessing and normalization settings as the unsupervised autoencoder.

We evaluate two supervised training setups. In the fully supervised configuration, the model is trained on all available attack classes. This setting

serves as a reference for upper bound performance given complete label information. The second setup is the leave-one-attack-out (LOAO) configuration, where a single attack type is iteratively removed from the training set and used exclusively for testing. This simulates a zero-day detection scenario and measures how well the model handles previously unseen attacks.

These supervised baselines enable direct comparison between discriminative learning and the reconstruction-based anomaly detection mechanisms of both classical and HQC autoencoders. Moreover, the inclusion of both the fully supervised and LOAO configurations provides complementary insight into the performance-robustness trade-off central to this study.

To ensure a fair comparison with supervised approaches, each LOAO experiment is evaluated only on samples containing normal traffic and the excluded attack category. This subset-based evaluation isolates the model’s ability to detect previously unseen attacks which removes the influence of classes encountered during training. For consistency, the unsupervised autoencoders are evaluated under the same per-attack splitting scheme, and the reported AUROC represents the mean across all held-out attack iterations. The fully supervised configuration remained evaluated on the full test set, as it represents an upper-bound reference. When comparing the classical and HQC autoencoders, however, we used the standard full test partitions to maintain consistency with prior unsupervised anomaly detection studies and to directly assess robustness across configurations.

3.6. Experimental Setup and Evaluation

We repeat each experiment 5 times with different random seeds. All models are implemented using JAX (Bradbury et al., 2018) and PennyLane (Bergholm et al., 2018) and trained using the Adam optimizer (Kingma and Ba, 2014) with a learning rate of 10^{-3} and a batch size of 256. Early stopping based on validation loss is employed to prevent overfitting. To ensure fair comparison, all supervised and unsupervised models share identical preprocessing, optimization settings, and evaluation metrics.

Performance is primarily evaluated using the AUROC. Results are reported as the mean and standard deviation across the 5 runs. To assess the statistical significance of performance differences between configurations, we employ paired t -tests with a significance level of 0.01.

3.7. Hardware Noise Simulation

To assess the practical viability of HQC models, we conduct a noise simulation study on the best-performing HQC architecture for the UNSW-NB15 dataset. We model the effect of coherent gate errors by applying a random $R_X(\epsilon)$ rotation after each gate in the variational circuit. The error term ϵ is drawn from a Gaussian distribution $\mathcal{N}(0, \sigma^2)$, where the standard deviation σ represents the noise level. This simulates a general-purpose error that introduces random rotations around the X-axis of the Bloch sphere, affecting both the amplitude and phase of the quantum state. We test performance at noise levels of $\sigma \in [0.0, 0.01, 0.03, 0.1, 0.3, 1.0]$.

This over-rotation model captures coherent errors observed on real quantum processors and allows direct mapping between σ and average gate infidelity. For single-qubit gates, the average fidelity is $F_{\text{avg}}(\sigma) = (2 + e^{-\sigma^2/2})/3$ (Nielsen, 2002), yielding infidelity $r(\sigma) = (1 - e^{-\sigma^2/2})/3$. Values of σ between 0.07 and 0.09 correspond to typical single-qubit error rates ($r \sim 10^{-3}$, or 0.1%) reported for IBM’s superconducting hardware (AbuGhanem, 2025), while $\sigma = 0.01$ corresponds to a near-future logical-qubit regime with $r \sim 10^{-5}$ (Smith et al., 2025). Thus, the chosen noise levels span the transition from present-day physical qubits to idealized logical-qubit performance.

3.8. Reproducibility

To ensure the reproducibility of our results and to facilitate future research, the source code and experimental configurations used in this study are publicly available at <https://github.com/arasyi/hqcae-network-intrusion-detection>.

4. Results and Discussion

In this section, we present the empirical evaluation of the HQC autoencoder framework. First, we compare the performance of the highest-achieving HQC and classical AE models and assess the sensitivity of each model family to its architectural configuration. Second, we compare the unsupervised AE models against supervised baselines, utilizing an LOAO protocol to assess performance in a simulated zero-day attack scenario. Third, we analyze the impact of core design choices within the autoencoder architecture on model performance. Finally, we assess the robustness of the HQC models to simulated hardware noise to determine their potential for practical deployment.

4.1. Performance Comparison and Sensitivity to Architectural Configuration

Our initial analysis compares the best-performing configurations from the classical and HQC model families. Table 2 reports the results, and the corresponding settings for each model are shown in Table 3.

The strongest HQC configurations achieve a mean AUROC of 0.9009 on UNSW-NB15 and 0.9611 on NSL-KDD. Although both values are higher than those of the classical baseline, the differences are not statistically significant ($p = 0.057$ and $p = 0.618$). On CIC-IDS2017, however, the classical model achieves a higher AUROC and the difference is found to be significant ($p < 0.01$). These results suggest that HQC models can match or surpass classical models, but their advantage is not consistent across datasets.

Next, we take a look at performance stability across different architectural choices. A key distinction is revealed by analyzing the full distribution of AUROC scores for all tested configurations, as visualized in Fig. 2. Notably, the classical models display a narrower range and a slightly higher median, which indicates lower sensitivity to architectural variations.

Observation 1. HQC models show substantially higher variance across architectural configurations, which reflects strong sensitivity to quantum-layer placement and measurement strategy.

Table 2: Comparison of the best Classical and HQC models per dataset by mean AUROC (five runs).

Metric	UNSW-NB15	NSL-KDD	CIC-IDS2017
Classical AUROC	$0.8976 \pm 0.0025^\dagger$	$0.9595 \pm 0.0036^\dagger$	$0.9424 \pm 0.0017^\dagger$
HQC AUROC	0.9009 ± 0.0029	0.9611 ± 0.0044	0.9361 ± 0.0039
Δ AUROC	$+0.0032$ (+0.36%)	$+0.0017$ (+0.17%)	-0.0063 (-0.67%)
99% CI	$[-0.0089, 0.0024]$	$[-0.0158, 0.0125]$	$[0.0004, 0.0123]$
p -value	0.0566	0.6183	0.0080
d_z	+1.1881	+0.2412	-2.1940
Significance	×	×	✓

4.2. Comparison to Supervised Baselines

To contextualize the performance of the unsupervised models, we compare them against a supervised baseline under two evaluation protocols: (i) a full

Table 3: Configurations for the best classical and HQC models reported in Table 2.

Dataset	Model Family	Top Architecture Configuration
UNSW-NB15	Classical	Classical AE (Recon. Error)
	HQC	HQCAE-Early-ExpVal (Latent Reg., Recon. Error)
NSL-KDD	Classical	Classical AE (Recon. Error)
	HQC	HQCAE-Early-Probs (Latent Reg., Recon. Error)
CIC-IDS2017	Classical	Classical AE (Recon. Error)
	HQC	HQCAE-Early-ExpVal (No Latent Reg., Recon. Error)

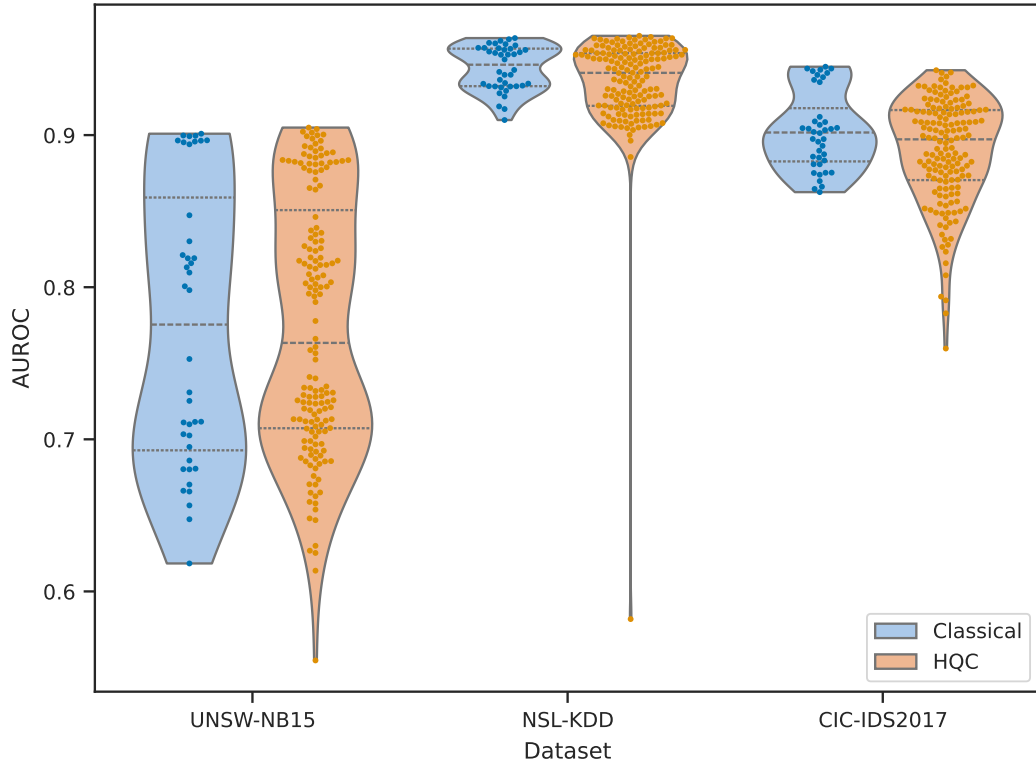


Figure 2: Violin and swarm plots of AUROC distributions for all classical and HQC configurations across the three datasets.

test set configuration, representing ideal conditions where all attack types are known during training, and (ii) an LOAO protocol that simulates zero-day scenarios by withholding one attack class at a time for testing. The results are summarized in Table 4.

Under the full test setting, the supervised classifier achieves the highest mean AUROC on UNSW-NB15 (0.9717) and CIC-IDS2017 (0.9991), establishing an empirical upper-bound reference when all threats are known in advance. However, its performance on NSL-KDD (0.8828) is notably lower, where both unsupervised models outperform it, indicating that even under complete data conditions, generalization is dataset dependent. Between the unsupervised models, the HQC autoencoder slightly outperforms the classical AE on UNSW-NB15 and NSL-KDD, while the classical AE remains marginally stronger on CIC-IDS2017.

The LOAO protocol is then employed to evaluate model performance against previously unseen threats to simulate zero-day attack scenarios. As can be seen in Table 4, the supervised models show a drastic decrease in performance, together with large standard deviations, e.g., 0.7596 ± 0.2706 on NSL-KDD. This variance, illustrated by the wide data distribution in Fig. 3, indicates that the model’s ability to detect novel threats is highly dependent on the characteristics of the unseen attack. This finding underscores the critical need for robust unsupervised methods for detecting novel intrusions.

In this realistic zero-day context, an analysis of performance variance across the held-out attack classes reveals key differences in model reliability. Both unsupervised models show substantially lower variance in AUROC scores compared to the supervised model. Interestingly, a direct comparison between the unsupervised approaches demonstrates that HQC models achieve higher average AUROC with lower variance than the classical ones. This finding contrasts with the results reported in Section 4.1, where HQC models are found to be more sensitive to architectural configuration as indicated by higher variance across configuration. On all three datasets, HQC models maintain consistently tighter AUROC distributions than their classical counterparts (see Fig. 3). For instance, on UNSW-NB15, the AUROC standard deviation for the HQC model is 0.1406, compared to 0.1645 for the classical model.

Observation 2. While HQC models are more sensitive to architectural choices during design, a well-configured HQC variant delivers more stable and reliable detection on unseen attack types compared to both classical supervised

and unsupervised model counterparts.

Table 4: AUROC comparison of supervised baselines and unsupervised autoencoders across datasets under full test and LOAO protocols.

Protocol	Model	UNSW-NB15	NSL-KDD	CIC-IDS2017
Full Test Set (All Attacks)	Supervised (Classical)	0.9717 \pm 0.0007 [†]	0.8828 \pm 0.0101	0.9991 \pm 0.0003 [†]
	Unsupervised (Classical)	0.8976 \pm 0.0025	0.9595 \pm 0.0036 [†]	0.9424 \pm 0.0017
	Unsupervised (HQC)	0.9009 \pm 0.0029	0.9611 \pm 0.0044	0.9361 \pm 0.0039
LOAO	Supervised (Classical)	0.9346 \pm 0.0665 [†]	0.7596 \pm 0.2706	0.8499 \pm 0.1935
	Unsupervised (Classical)	0.8326 \pm 0.1645	0.9448 \pm 0.0470	0.8462 \pm 0.1383
	Unsupervised (HQC)	0.8449 \pm 0.1406	0.9486 \pm 0.0424 [†]	0.8488 \pm 0.1321 [†]

Table 5: Statistical analysis of HQC autoencoder design factors.

Factor	Conditions	AUROC ($\mu \pm \sigma$)	Δ (1 st –2 nd)	99% CI	p	d_z	Sig.
Detection Mechanism	Recon. Error Thresholding	0.9043 \pm 0.0576	0.0759	[0.0647, 0.0872]	0.0000	1.1314	✓
	Downstream Model (IF)	0.8283 \pm 0.0954					
Variational Objective	Standard AE	0.8773 \pm 0.0839	0.0221	[0.0145, 0.0298]	0.0000	0.4843	✓
	VAE	0.8552 \pm 0.0895					
Latent Regularization	Without Regularization	0.8685 \pm 0.0853	0.0045	[-0.0017, 0.0107]	0.0605	0.1217	×
	With Regularization	0.8640 \pm 0.0895					
QLayer Placement	Early Stage	0.8730 \pm 0.0856	0.0133	[0.0069, 0.0198]	0.0000	0.3450	✓
	Late Stage	0.8596 \pm 0.0888					
QLayer Measurement	Expectation Value	0.8658 \pm 0.0888	-0.0010	[-0.0075, 0.0055]	0.6971	-0.0252	×
	Probabilities	0.8668 \pm 0.0861					

4.3. Analysis of Autoencoder Design Choices

The preceding analysis shows that the performance and reliability of HQC models are strongly influenced by architectural configuration. To better understand these dependencies, this section examines how key design factors, such as quantum-layer placement and measurement scheme, affect model performance. Statistical comparisons using paired t -tests are conducted all HQC configurations to evaluate the impact of each factor on mean AUROC, as summarized in Table 5. To assess whether the observed differences are meaningful, we performed paired t -tests on run-level AUROC across five matched runs, using $p < 0.01$ as the threshold for significance.

4.3.1. Anomaly Detection Mechanism

Within HQC configurations, using the reconstruction error directly as the anomaly score produces significantly larger mean AUROC than applying an isolation forest to the latent space. This trend mirrors the behavior

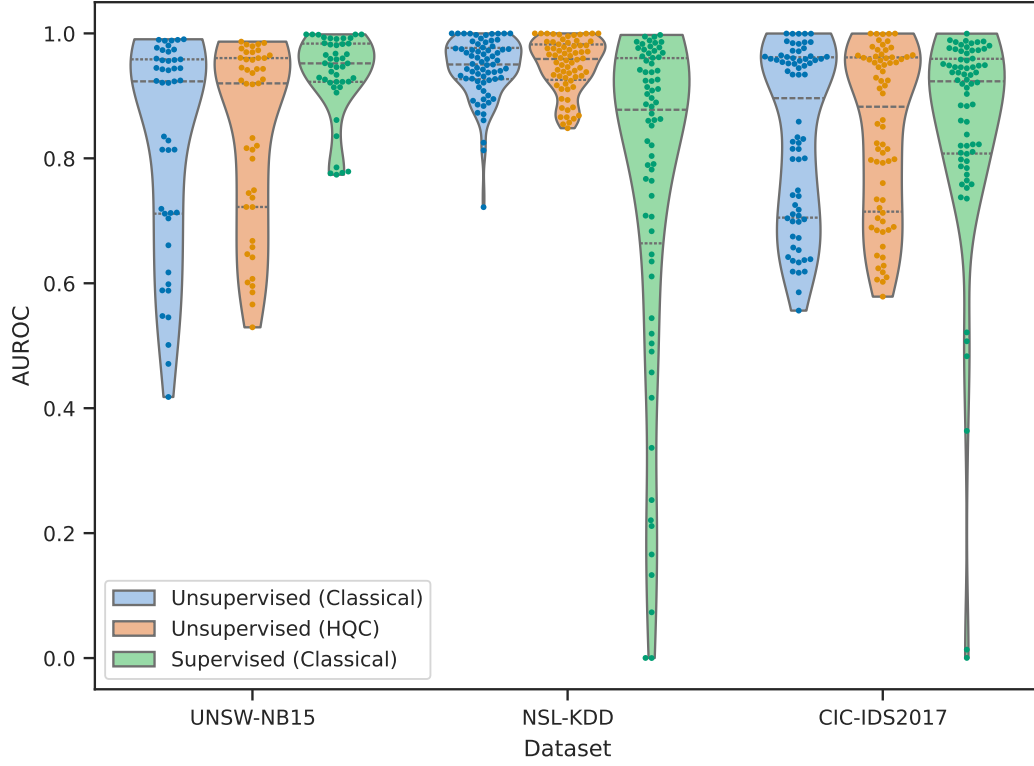


Figure 3: Violin and swarm plots of AUROC for models under the LOAO protocol.

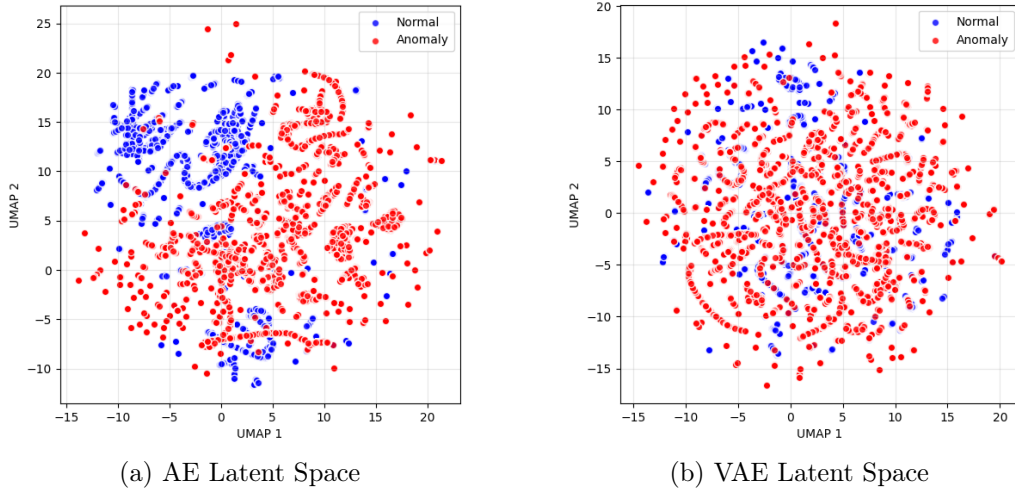


Figure 4: UMAP visualization of an autoencoder’s latent space on the NSL-KDD test set.

of classical autoencoders and reflects the close alignment between the training objective, namely minimization of reconstruction loss, and the detection metric. Although not a quantum-specific effect, this result confirms that the introduction of quantum layers does not alter this fundamental relationship.

4.3.2. *Observed Effect of the Variational Objective*

Incorporating a variational objective in the form of a KL-divergence regularization term ($\beta > 0$ in Eq. 5) is associated with a statistically significant reduction in mean performance as shown in Table 5. UMAP (McInnes et al., 2018) visualizations, shown in Fig. 4, indicate that the latent representations learned under the variational constraint tend to form less separable clusters than those of standard HQC autoencoders. While this suggests that strong regularization may limit discriminative capacity in this specific anomaly detection setting, further investigation is needed to determine whether this behavior generalizes across datasets or VAE formulations.

4.3.3. *Efficacy of Latent Space Regularization*

Latent regularization (Nkashama et al., 2024) showed no statistically significant effect on mean AUROC across HQC. While some top-performing HQC architectures employed this regularization as shown in Table 3, its impact is inconsistent across datasets.

4.3.4. *HQC Layer Architecture.*

The design of the HQC layer, especially its position within the encoder, has a strong influence on model performance.

Statistical analysis indicates that placing the quantum layer early in the encoder yields significantly better results than a late-stage placement as shown in Table 5. The early-stage configuration processes higher-dimensional inputs through amplitude embedding, allowing the PQC to operate on richer feature representations before information is lost through classical dimensionality reduction. This likely allows the model to capture more complex data correlations that are harder to recover once the representation has been reduced.

Although the measurement scheme does not show a statistically significant effect ($p = 0.697$), we observe a nominal crossover trend when it is considered together with the quantum layer placement. The probability readout yields a slightly higher mean AUROC for early-stage integration (0.8750 ± 0.0804), which is consistent with the idea that its high-dimensional

feature output can exploit structure present in the raw input space. Conversely, the expectation value readout performs nominally better when the quantum layer is placed later in the encoder (0.8607 ± 0.0869), suggesting its compact feature acts more effectively as a bottleneck once classical features have already been compressed. Given the large standard deviations ($\sigma \approx 0.09$), this pattern must be viewed as a preliminary trend and broader experiments are needed to confirm its generalization across architectures.

Table 6: Mean AUROC for combinations of quantum-layer placement and measurement scheme

Placement	Expectation Value	Probabilities
Early	0.8709 ± 0.0911	0.8750 ± 0.0804
Late	0.8607 ± 0.0869	0.8586 ± 0.0913

4.4. Impact of Simulated Hardware Noise on HQC Performance

We examine the top-performing configuration under simulated coherent gate errors in order to determine the HQC models’ practicality for deployment on near-term quantum hardware. The results, shown in Fig. 5, quantify the challenge posed by hardware noise. At a very low noise level of $\sigma = 0.01$ (corresponding to a per-gate infidelity of about 1.7×10^{-5} , well below current hardware capabilities), the model’s AUROC drops by 2.68%, already falling below the performance of the best classical model. Performance continues to degrade as noise increases. This degradation highlights the importance of quantum error mitigation and noise-aware algorithm design for transitioning HQC models from simulation to practical deployment (Cai et al., 2023; Quek et al., 2024).

5. Conclusion and Future Work

This study presents a systematic and large-scale evaluation of unsupervised autoencoders (classical and HQC) alongside supervised baselines for network intrusion detection. To our knowledge, it offers the first quantitative characterization of HQC autoencoder behavior for NIDS and provides data-driven evidence on how architectural and hardware factors may shape performance in quantum-enhanced network defense systems.

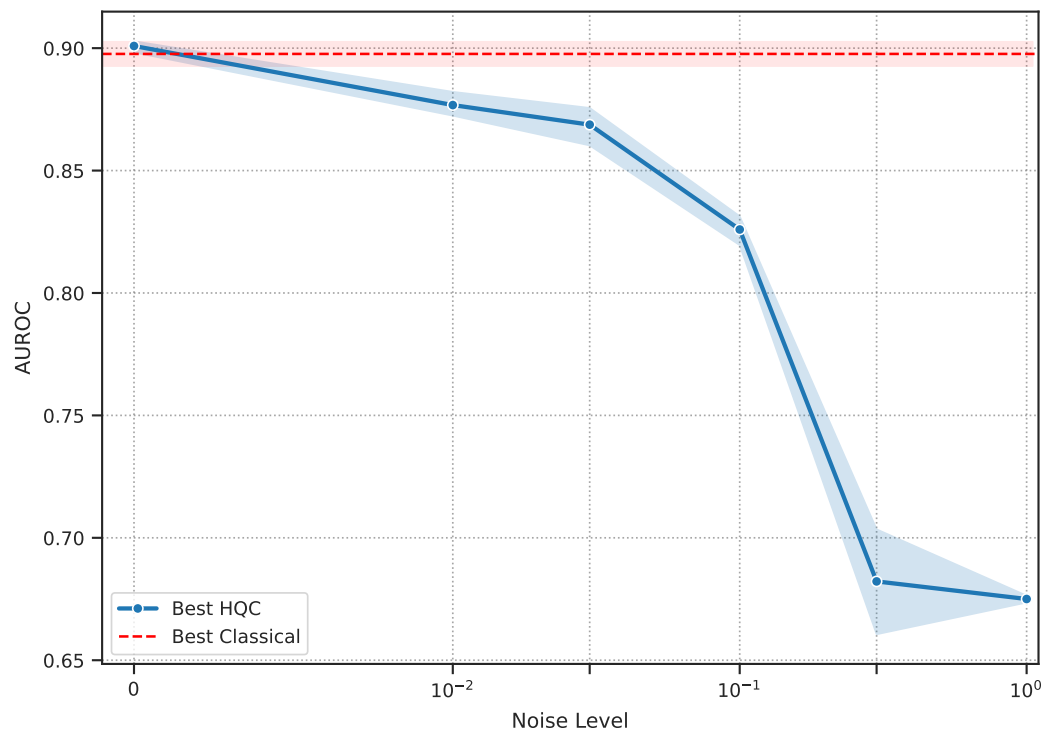


Figure 5: Impact of simulated coherent gate error on AUROC for the best HQC model on UNSW-NB15.

Our results indicate that classical AEs tend to show less variation in performance across architectural configurations. HQC models behave differently. When evaluated in their best-performing configurations under the LOAO protocol, they achieve higher mean AUROC and lower variability across held-out attack classes. This suggests that HQC models may generalize more effectively to unseen attacks than both classical unsupervised and supervised approaches on the benchmark datasets.

At the same time, the experiments reveal a trade-off. HQC performance depends heavily to architectural choices and require careful tuning. In favorable configurations, however, they appear more stable and reliable against novel threats. Simulated gate noise experiments further indicate that HQC performance can decline significantly even at relatively low noise levels, underscoring the importance of noise-aware training and error mitigation strategies for any realistic near-term deployment.

Future research can extend this work along several technically grounded directions. One natural step is to execute the identified HQC architectures on NISQ hardware in combination with quantum error mitigation strategies (Cai et al., 2023), which would allow empirical testing of the simulated relationship between noise and performance. Another direction is the development of noise resilient HQC architectures that are co-designed with the target hardware and that make explicit use of device specific constraints (Quek et al., 2024), with the aim of further stabilizing model variance. It may also be beneficial to explore advanced quantum ansatzes, for example quantum convolutional neural networks (Cong et al., 2019) or graph-informed circuit families, to improve representational expressivity for structured network data. Finally, the scalability of HQC models with respect to growing qubit counts and more efficient data embedding strategies (Aaronson, 2015; Cerezo et al., 2021) remains an open and practically important question for deployment at realistic network scales.

References

- Aaronson, S., 2015. Read the fine print. *Nature Physics* 11, 291–293. doi:10.1038/nphys3272.
- Abreu, D., Rothenberg, C.E., Abelem, A., 2024. QML-IDS: Quantum machine learning intrusion detection system, in: *2024 IEEE Symposium on Computers and Communications (ISCC)*, IEEE, Paris, France. pp. 1–6. doi:10.1109/ISCC61673.2024.10733655, arXiv:2410.16308.

- AbuGhanem, M., 2025. IBM quantum computers: Evolution, performance, and future directions. *Journal of Supercomputing* 81, 687. doi:10.1007/s11227-025-07047-7, arXiv:2410.00916.
- Al Siam, A., Alazab, M., Awajan, A., Faruqui, N., 2025. A comprehensive review of AI's current impact and future prospects in cybersecurity. *IEEE Access* 13, 14029–14050. doi:10.1109/ACCESS.2025.3528114.
- Alsoufi, M.A., Razak, S., Siraj, M.M., Nafea, I., Ghaleb, F.A., Saeed, F., Nasser, M., 2021. Anomaly-based intrusion detection systems in IoT using deep learning: A systematic literature review. *Applied Sciences* 11, 8383. doi:10.3390/app11188383.
- An, J., Cho, S., 2015. Variational autoencoder based anomaly detection using reconstruction probability. *Special Lecture on IE* 2, 1–18.
- Asharf, J., Moustafa, N., Khurshid, H., Debie, E., Haider, W., Wahab, A., 2020. A Review of Intrusion Detection Systems Using Machine and Deep Learning in Internet of Things: Challenges, Solutions and Future Directions. *Electronics* 9, 1177. doi:10.3390/electronics9071177.
- Bergholm, V., Izaac, J., Schuld, M., Gogolin, C., Ahmed, S., Ajith, V., Alam, M.S., Alonso-Linaje, G., AkashNarayanan, B., Asadi, A., Arrazola, J.M., Azad, U., Banning, S., Blank, C., Bromley, T.R., Cordier, B.A., Ceroni, J., Delgado, A., Di Matteo, O., Dusko, A., Garg, T., Guala, D., Hayes, A., Hill, R., Ijaz, A., Isacsson, T., Ittah, D., Jahangiri, S., Jain, P., Jiang, E., Khandelwal, A., Kottmann, K., Lang, R.A., Lee, C., Loke, T., Lowe, A., McKiernan, K., Meyer, J.J., Montañez-Barrera, J.A., Moyard, R., Niu, Z., O’Riordan, L.J., Oud, S., Panigrahi, A., Park, C.Y., Polatajko, D., Quesada, N., Roberts, C., Sá, N., Schoch, I., Shi, B., Shu, S., Sim, S., Singh, A., Strandberg, I., Soni, J., Száva, A., Thabet, S., Vargas-Hernández, R.A., Vincent, T., Vitucci, N., Weber, M., Wierichs, D., Wiersema, R., Willmann, M., Wong, V., Zhang, S., Killoran, N., 2018. PennyLane: Automatic differentiation of hybrid quantum-classical computations. doi:10.48550/ARXIV.1811.04968.
- Biamonte, J., Wittek, P., Pancotti, N., Rebentrost, P., Wiebe, N., Lloyd, S., 2017. Quantum machine learning. *Nature* 549, 195–202. doi:10.1038/nature23474.

- Bouman, R., Heskes, T., 2025. Autoencoders for anomaly detection are unreliable. doi:10.48550/arXiv.2501.13864, arXiv:2501.13864.
- Bradbury, J., Frostig, R., Hawkins, P., Johnson, M.J., Leary, C., Maclaurin, D., Necula, G., Paszke, A., VanderPlas, J., Wanderman-Milne, S., Zhang, Q., 2018. JAX: Composable transformations of Python+NumPy programs.
- Cai, Z., Babbush, R., Benjamin, S.C., Endo, S., Huggins, W.J., Li, Y., McClean, J.R., O’Brien, T.E., 2023. Quantum error mitigation. *Reviews of Modern Physics* 95, 45005. doi:10.1103/RevModPhys.95.045005.
- Cerezo, M., Arrasmith, A., Babbush, R., Benjamin, S.C., Endo, S., Fujii, K., McClean, J.R., Mitarai, K., Yuan, X., Cincio, L., Coles, P.J., 2021. Variational quantum algorithms. *Nature Reviews Physics* 3, 625–644. doi:10.1038/s42254-021-00348-9.
- Chen, J., Zhou, H., Mei, Y., Adam, G., Bastian, N.D., Lan, T., 2023. Real-time Network Intrusion Detection via Decision Transformers. doi:10.48550/arXiv.2312.07696, arXiv:2312.07696.
- Cong, I., Choi, S., Lukin, M.D., 2019. Quantum convolutional neural networks. *Nature Physics* 15, 1273–1278. doi:10.1038/s41567-019-0648-8.
- Frehner, R., Stockinger, K., 2025. Applying quantum autoencoders for time series anomaly detection. *Quantum Machine Intelligence* 7, 59. doi:10.1007/s42484-025-00285-1.
- Gouveia, A., Correia, M., 2020. Towards quantum-enhanced machine learning for network intrusion detection, in: 2020 IEEE 19th International Symposium on Network Computing and Applications (NCA), IEEE, Cambridge, MA, USA. pp. 1–8. doi:10.1109/NCA51143.2020.9306691.
- Guerra, J.L., Catania, C., Veas, E., 2022. Datasets are not enough: Challenges in labeling network traffic. *Computers & Security* 120, 102810. doi:10.1016/j.cose.2022.102810.
- Guo, Y., 2023. A review of machine learning-based zero-day attack detection: Challenges and future directions. *Computer Communications* 198, 175–185. doi:10.1016/j.comcom.2022.11.001.

- Havlíček, V., Córcoles, A.D., Temme, K., Harrow, A.W., Kandala, A., Chow, J.M., Gambetta, J.M., 2019. Supervised learning with quantum-enhanced feature spaces. *Nature* 567, 209–212. doi:10.1038/s41586-019-0980-2.
- Hdaib, M., Rajasegarar, S., Pan, L., 2024. Quantum deep learning-based anomaly detection for enhanced network security. *Quantum Machine Intelligence* 6, 26. doi:10.1007/s42484-024-00163-2.
- Jerbi, S., Fiderer, L.J., Poulsen Nautrup, H., Kübler, J.M., Briegel, H.J., Dunjko, V., 2023. Quantum machine learning beyond kernel methods. *Nature Communications* 14, 517. doi:10.1038/s41467-023-36159-y.
- Kingma, D.P., Ba, J., 2014. Adam: A Method for Stochastic Optimization. doi:10.48550/ARXIV.1412.6980.
- Kingma, D.P., Welling, M., 2013. Auto-Encoding Variational Bayes. doi:10.48550/ARXIV.1312.6114.
- Larocca, M., Thanasilp, S., Wang, S., Sharma, K., Biamonte, J., Coles, P.J., Cincio, L., McClean, J.R., Holmes, Z., Cerezo, M., 2025. Barren plateaus in variational quantum computing. *Nature Reviews Physics* 7, 174–189. doi:10.1038/s42254-025-00813-9, arXiv:2405.00781.
- LaRose, R., Coyle, B., 2020. Robust data encodings for quantum classifiers. *Physical Review A* 102, 32420. doi:10.1103/PhysRevA.102.032420.
- Liu, F.T., Ting, K.M., Zhou, Z.H., 2008. Isolation forest, in: 2008 Eighth IEEE International Conference on Data Mining, IEEE, Pisa, Italy. pp. 413–422. doi:10.1109/icdm.2008.17.
- Liu, L., Engelen, G., Lynar, T., Essam, D., Joosen, W., 2022. Error prevalence in NIDS datasets: A case study on CIC-IDS-2017 and CSE-CIC-IDS-2018, in: 2022 IEEE Conference on Communications and Network Security (CNS), IEEE, Austin, TX, USA. pp. 254–262. doi:10.1109/CNS56114.2022.9947235.
- Lo, W.W., Layeghy, S., Sarhan, M., Gallagher, M., Portmann, M., 2022. E-GraphSAGE: A graph neural network based intrusion detection system for IoT, in: NOMS 2022-2022 IEEE/IFIP Network Operations and Management Symposium, IEEE, Budapest, Hungary. pp. 1–9. doi:10.1109/NOMS54207.2022.9789878.

- Long, Z., Yan, H., Shen, G., Zhang, X., He, H., Cheng, L., 2024. A transformer-based network intrusion detection approach for cloud security. *Journal of Cloud Computing* 13, 5. doi:10.1186/s13677-023-00574-9.
- Manocchio, L.D., Layeghy, S., Lo, W.W., Kulatilleke, G.K., Sarhan, M., Portmann, M., 2024. FlowTransformer: A transformer framework for flow-based network intrusion detection systems. *Expert Systems with Applications* 241, 122564. doi:10.1016/j.eswa.2023.122564.
- McInnes, L., Healy, J., Melville, J., 2018. UMAP: Uniform Manifold Approximation and Projection for Dimension Reduction. doi:10.48550/ARXIV.1802.03426.
- Mitarai, K., Negoro, M., Kitagawa, M., Fujii, K., 2018. Quantum circuit learning. *Physical Review A* 98, 32309. doi:10.1103/PhysRevA.98.032309.
- Mottonen, M., Vartiainen, J.J., Bergholm, V., Salomaa, M.M., 2004. Transformation of quantum states using uniformly controlled rotations.
- Moustafa, N., Slay, J., 2015. UNSW-NB15: A comprehensive data set for network intrusion detection systems (UNSW-NB15 network data set), in: 2015 Military Communications and Information Systems Conference (MilCIS), IEEE, Canberra, Australia. pp. 1–6. doi:10.1109/MilCIS.2015.7348942.
- Neloy, A.A., Turgeon, M., 2024. A comprehensive study of auto-encoders for anomaly detection: Efficiency and trade-offs. *Machine Learning with Applications* 17, 100572. doi:10.1016/j.mlwa.2024.100572.
- Ngairangbam, V.S., Spannowsky, M., Takeuchi, M., 2022. Anomaly detection in high-energy physics using a quantum autoencoder. *Physical Review D* 105, 95004. doi:10.1103/PhysRevD.105.095004.
- Nielsen, M.A., 2002. A simple formula for the average gate fidelity of a quantum dynamical operation. *Physics Letters A* 303, 249–252. doi:10.1016/S0375-9601(02)01272-0, arXiv:quant-ph/0205035.
- Nkashama, D.K., Félicien, J.M., Soltani, A., Verdier, J.C., Tardif, P.M., Frappier, M., Kabanza, F., 2024. Deep learning for network anomaly

- detection under data contamination: Evaluating robustness and mitigating performance degradation. doi:10.48550/ARXIV.2407.08838.
- Pinto, D., Amorim, I., Maia, E., Praça, I., 2025. A novel approach to network traffic analysis: The HERA tool. doi:10.48550/ARXIV.2501.07475.
- Preskill, J., 2018. Quantum computing in the NISQ era and beyond. *Quantum* 2, 79. doi:10.22331/q-2018-08-06-79.
- Quek, Y., Stilck França, D., Khatri, S., Meyer, J.J., Eisert, J., 2024. Exponentially tighter bounds on limitations of quantum error mitigation. *Nature Physics* 20, 1648–1658. doi:10.1038/s41567-024-02536-7.
- Sakhnenko, A., O’Meara, C., Ghosh, K.J.B., Mendl, C.B., Cortiana, G., Bernabé-Moreno, J., 2022. Hybrid classical-quantum autoencoder for anomaly detection. *Quantum Machine Intelligence* 4, 27. doi:10.1007/s42484-022-00075-z.
- Sakurada, M., Yairi, T., 2014. Anomaly detection using autoencoders with nonlinear dimensionality reduction, in: *Proceedings of the MLSDA 2014 2nd Workshop on Machine Learning for Sensory Data Analysis*, ACM, Gold Coast Australia QLD Australia. pp. 4–11. doi:10.1145/2689746.2689747.
- Schuld, M., Bocharov, A., Svore, K.M., Wiebe, N., 2020. Circuit-centric quantum classifiers. *Physical Review A* 101, 32308. doi:10.1103/PhysRevA.101.032308.
- Schuld, M., Sweke, R., Meyer, J.J., 2021. Effect of data encoding on the expressive power of variational quantum-machine-learning models. *Physical Review A* 103, 32430. doi:10.1103/PhysRevA.103.032430.
- Sharafaldin, I., Habibi Lashkari, A., Ghorbani, A.A., 2018. Toward generating a new intrusion detection dataset and intrusion traffic characterization:, in: *Proceedings of the 4th International Conference on Information Systems Security and Privacy*, SCITEPRESS - Science and Technology Publications, Funchal, Madeira, Portugal. pp. 108–116. doi:10.5220/0006639801080116.

- Sharma, S., Chen, Z., 2024. A systematic study of adversarial attacks against network intrusion detection systems. *Electronics* 13, 5030. doi:10.3390/electronics13245030.
- Shende, V., Bullock, S., Markov, I., 2006. Synthesis of quantum-logic circuits. *IEEE Transactions on Computer-Aided Design of Integrated Circuits and Systems* 25, 1000–1010. doi:10.1109/TCAD.2005.855930.
- Smith, M.C., Leu, A.D., Miyanishi, K., Gely, M.F., Lucas, D.M., 2025. Single-qubit gates with errors at the 10^{-7} level. *Physical Review Letters* 134, 230601. doi:10.1103/42w2-6ccy.
- Sun, Z., Teixeira, A.M., Toor, S., 2024. GNN-IDS: Graph neural network based intrusion detection system, in: *Proceedings of the 19th International Conference on Availability, Reliability and Security*, ACM, Vienna Austria. pp. 1–12. doi:10.1145/3664476.3664515.
- Tavallae, M., Bagheri, E., Lu, W., Ghorbani, A.A., 2009. A detailed analysis of the KDD CUP 99 data set, in: *2009 IEEE Symposium on Computational Intelligence for Security and Defense Applications*, IEEE, Ottawa, ON, Canada. pp. 1–6. doi:10.1109/CISDA.2009.5356528.
- Vinayakumar, R., Alazab, M., Soman, K.P., Poornachandran, P., Al-Nemrat, A., Venkatraman, S., 2019. Deep learning approach for intelligent intrusion detection system. *IEEE Access* 7, 41525–41550. doi:10.1109/ACCESS.2019.2895334.
- Wu, Y., Zou, B., Cao, Y., 2024. Current status and challenges and future trends of deep learning-based intrusion detection models. *Journal of Imaging* 10, 254. doi:10.3390/jimaging10100254.
- Yin, C., Zhu, Y., Fei, J., He, X., 2017. A deep learning approach for intrusion detection using recurrent neural networks. *IEEE Access* 5, 21954–21961. doi:10.1109/ACCESS.2017.2762418.
- Yu, J., Oh, H., Kim, M., Kim, J., 2021. Normality-calibrated autoencoder for unsupervised anomaly detection on data contamination. doi:10.48550/arXiv.2110.14825, arXiv:2110.14825.

- Zachos, G., Essop, I., Mantas, G., Porfyraakis, K., Ribeiro, J.C., Rodriguez, J., 2021. An anomaly-based intrusion detection system for internet of medical things networks. *Electronics* 10, 2562. doi:10.3390/electronics10212562.
- Zhong, M., Lin, M., Zhang, C., Xu, Z., 2024. A survey on graph neural networks for intrusion detection systems: Methods, trends and challenges. *Computers & Security* 141, 103821. doi:10.1016/j.cose.2024.103821.